ISSN 1330-3651 (Print), ISSN 1848-6339 (Online)
https://doi.org/10.17559/TV-20240322001425
Original scientific paper

Influence of p-MIG Welding Parameters to Wall Geometry of Aluminium Alloy 2319 Fabricated Using WAAM

Živko JURIŠIĆ*, Nikša KRNIĆ

Abstract: Arc welding processes are used in additive manufacturing today, adding thin layers of metal according to a programmed heat source path. This paper presents a study of the influence of robotic p-MIG process parameters on wall geometry made of aluminium alloy 2319. Experimental methodology was based on variation of arc travel speed (6, 7, 8 mm/s), with constant heat input per layer length and suitable arc power. The selected heat input per layer length for the first layer was 265 J/mm ± 5%, and for the other layers it was 217 J/mm ± 5%. The analysis of wall geometry, layer height and width, considering deposition efficiency and surface waviness index, was applied in the research. The results showed that same heat input with different WAAM process parameters yielded different wall geometries and wall geometry quality. 3D model of the wall geometry proved to be a useful tool for volume and deposition efficiency calculations. Moreover, the graphical display and interpretation of the standard deviation shows the level of stability of the geometric features of the wall layers. Based on the implemented methodology, an appropriate selection of process parameters is given to achieve the most efficient wall geometry of aluminium alloy 2319.

Keywords: aluminium alloy 2319; deposition efficiency; heat input; p-MIG welding parameters; wall geometry; wire arc additive manufacturing

1 INTRODUCTION

According to the definition of the American Society for Testing and Materials, additive manufacturing is the process of joining materials to create objects from 3D models, usually layer by layer, unlike subtractive and formative manufacturing methodologies [1].

Technological processes that are most often applied in additive manufacturing use a laser, an electric arc, plasma arc or an electron beam as a heat source [2]. The Wire arc additive manufacturing (WAAM) technology of metal parts uses electric arc processes such as GMAW (Gas Metal Arc Welding, also called in literature as MIG/MAG (Metal Inert Gas/Metal Active Gas) welding), TIG (Tungsten Inert Gas), CMT (Cold Metal Transfer) as a version of GMAW process and PAW (Plasma Arc Welding) [3]. One of the most common processes used in additive manufacturing of aluminium alloys is CMT process, due to relatively low heat input, controlled metal deposition, more efficient wire melting and high wire feed speed, comparable to the conventional GMAW process [4]. Many scientists study the influence of process parameters on the geometric features of multilayer walls, as well as on the microstructure, mechanical properties and irregularities that occur during additive manufacturing. The key process parameters that affect the properties of the fabricated part are welding current, arc voltage and arc travel speed. Terms such as heat input per layer length, arc power and the ratio of the wire feed speed and the travel speed (WFS/TS ratio) are derived from the mentioned parameters. Dimensional accuracy, deposition efficiency and surface waviness index are used as criteria for evaluation of the quality of the wall geometry. An overview of the issues of wire arc additive manufacturing using the GMAW process, with review of the influence of process parameters on the uniformity of the geometry and surface, and dimensional accuracy is given in the paper [5]. The basic mathematical terms for calculating the wall geometry are presented in the paper [6]. The proposed nonlinear model for the deposited layer geometry of thin walls is based on process parameters, physical variables and Rosenthal solution of temperature distribution. Thermal simulation using the finite element method, applied to aluminium alloy 5356 [7]. The influence of heat input as a key factor on the geometric features, mechanical properties and microstructure of the wall, during the successive deposition of layers is described in [8]. Multiple cycles of joining and solidification accumulate heat input, which affects the shape and volume of the layer. Since the WAAM process involves partial melting of the previous layer, improper control of the heat input can cause it to flow in the joining zone. The concept of heat management from the point of view of occurrence of irregularities, process planning, the influence of process parameters on the geometric features of the walls is given in the paper [9]. The majority of research is concerned with additive technology of steel and aluminium alloys. Among them, influence of different heat inputs, WFS/TS ratio and the other process parameters on wall geometry of steel alloys, calculating deposition efficiency, surface waviness index, standard error, and standard deviation of wall geometry, were investigated in [9-11]. Studying the application of WAAM process with aluminium alloys is still a challenge for many scientists. To achieve uniform geometry using the CMT process and 2319 aluminium alloy, different metal deposition strategies were applied such as deposition with (circling path) or without torch oscillation (bidirectional path) [12, 13]. The uniformity of the wall geometry using the parameter sets with different heat inputs (67,94 J/mm to 106,8 J/mm), was studied in [15]. The aim of the research with the double-pulse MIG process and ER5356 aluminium alloy was reducing heat input to obtain uniform geometry application of two techniques welding current reducing and travel speed increasing. The travel speed increasing technique led to instability of bead formation and bead humping. The application of cold metal transfer (CMT) process with different process variations (CMT, CMT-ADV (CMT advanced), CMT-P (CMT pulse) and CMT-PADV (CMT pulse advanced)) through the investigation of the influence of heat input (from 144 J/mm to 193 J/mm) on geometrical features of the wall of aluminium alloy wire 5556 (AlMg5Mn), diameter 1 mm, was discussed in the paper [16]. The multi-layered walls were produced by alternating direction strategy. Calculated

surface irregularity (SI) of the wall was from 0,89 mm to 1,4 mm and the material utilization (MU) was from 73% to 80%. The influence of heat input, welding current and arc voltage ratio on weld geometry was investigated in paper [17]. Experiments to produce 15-layer walls were performed with aluminium wire ER5356, using the CMT process with nine different parameter sets and constant arc travel speed. The range of heat input was from 270 J/mm to 460 J/mm. The achieved maximum deposition efficiency was 76%. The deposition efficiency of 91,12%, as the ratio of the effective volume and total volume, was calculated in application of hybrid laser-MIG process, with different laser powers for fabricating aluminium alloy 5356 walls [18]. The purpose of the investigation was analysing the laser power influence the wall geometry consisted of 20 layers produced in bidirectional direction. The MIG process parameters were constant. The width of each wall became stable after deposition of 5 - 6 layers due to faster heat dissipation through the substrate. One of the common appearances of geometric irregularity in welding process is humping, a phenomenon described by some authors [19, 20]. The desired wall geometry, without humping, can be achieved with a minimum surface waviness index, and travel speeds within the minimum and maximum limits [21]. The applied process for unidirectional depositing of 15-layer walls were CMT with the selected wire ER5356, diameter 1,2 mm, with lower travel speed of 42 cm/min and the upper travel speed of 175 cm/min. Calculated heat inputs were from 127,6 J/mm to 203,6 J/mm. In that research, as a measure of surface quality, calculated SWI (Surface Waviness Indexes) were 0,3 - 0,5 mm. Some authors applied techniques for optimizing process parameters, with the aim of achieving uniform wall geometry along the whole length of the layer. The model of artificial neural networks for predicting the weld geometry, which could be used in the study of the geometry of the first layer of the wall was applied in [22]. Some techniques were based on gradient adjustment of current, arc voltage, travel speed and applied to steel alloys. The adjustments of welding parameters in the arc striking and the arc extinguishing area of multi-layered wall were applied and showed significant improvement of uniform wall height [23]. In that study, the material of wire was copper-coated steel and MAG process was used for deposition. Three different optimization methods were applied with the aim of investigating dimensional irregularities at the beginning and end parts of single beads [24]. The material of the wire was ER100. The improvement strategy was a combination, varying TS configuration for the beginning part and extra return path for the end part of the layer. In paper [25], a strategy is given, which combines the control of parameters in the arc-striking and arc-extinguishing area with the control of the current in successive layers, while maintaining a constant heat input profile (660 J/mm). Different sets of parameters were used in the first six layers. After equilibrium was achieved, the subsequent layers were deposited using the last set of parameters. A total of 48 layers were deposited using MAG process with low alloy steel wire, ER70S-6. The achieved effective area is 96,8% of the total lateral area, and the deposition efficiency is 92,1%. The influence of main parameters of CMT process on geometric features of aluminium alloy 4043 wall obtained from WAAM technology was investigated, with the aim of achieving good geometric accuracy [26]. Multilayer deposition of 100 layers was evaluated by the calculation of standard deviation of layers width. Optimization of process parameters (pulse current and duration) improved geometric accuracy. The strategy of wall deposition height monitoring was successfully applied using visual inspection sensors of the previous and current layer [27]. To improve the geometric accuracy using the CMT process, a feedback control system was developed, which optimized the width and height of the layer [28]. A laser sensor was used to measure the geometry of the deposited layer and based on this data the system determined travel speeds for the next layer.

Based on the aforementioned published literature, it is concluded that research into the geometric characteristics of walls in the field of WAAM technology has included aluminium alloys such as 5356 (AlMg5), 5556 (AlMg5Mn), 4043 (Al-Si) and to a lesser extent 2319 (Al-Cu). Regarding aluminium alloy 2319, there is not enough detailed data with results relating to MIG process parameters and the wall geometry. A review of the published works reveals that processes such as MIG, CMT, double pulse MIG and the hybrid laser-MIG are most often used in WAAM technology of aluminium alloys. In the experiments, the used heat inputs were in the range 67,94 J/mm to 460 J/mm. In order to achieve a uniform geometry, different deposition strategies were applied unidirectional, bidirectional, circling deposition and optimization of process parameters. The quality criteria of the geometry of produced walls were deposition efficiency, SWI, standard error and standard deviation of geometric features. The achieved deposition efficiencies ranged from 76% to 91,12%, and the achieved SWI ranged from 0,3 mm to 1,4 mm. The uniformity of the wall geometry was considered adjusting the parameters in both parts of the layer, applying bidirectional deposition strategy, the return path in the end part of the layer and selecting different parameters in the first six layers.

In this study, considering previous researches in the field of WAAM technology of aluminium alloys, the experimental strategy was performed to produce aluminium alloy 2319 walls using pulse MIG (p-MIG) process. The strategy of this research was the bidirectional deposition of layers at three arc travel speeds and constant heat input. Due to the influence of heat removal through the substrate, different process parameters were selected for the first layer and the other layers.

Based on these experiments, the aim was to investigate the geometry of the first layer and the wall through the analysis of geometric features, width and height, and to examine the uniformity of geometry by the standard deviation of layers and the distribution of the wall geometry with respect to the possible occurrence of humping. By calculating the deposition efficiency, SWI and mass, the quality of the manufactured walls was determined. Also, the width and height in the beginning and the end parts of the walls were analysed, considering the deviation from quasi-stationary part.

2 MATERIALS AND METHODS

In this chapter, the materials and methodology of research are described, with the aim of analysing the geometric features of the walls produced by the WAAM process.

2.1 Experimental Setup

The experimental part of the research was performed in the Welding laboratory of the Department of Mechanical Engineering Technology, FESB, Split, by robotic welding cell for MIG/MAG welding (Fig. 1).

The following equipment was used:
- Robotic cell ABB, type IRB 1600 M2004.
- Control unit, ABB, type IRC5 M2004.
- Flexpendant controller for programming the movement of the robotic cell.
- Welding power source for MIG/MAG welding, Fronius, type TPS 4000R.
- Remote control unit of welding power source, RCU 5000i.
- Personal computer for data processing.

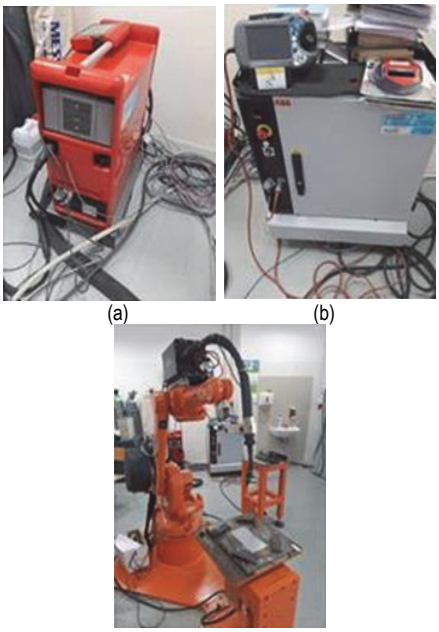

(a) (b) (c)

Figure 1 Robotic system for WAAM technology
a) welding power source; b) control unit; c) robot arm

Table 1 The chemical composition of wire Al 2319, [29]

El.	Mg	Ti	Mn	Zr	Cu	Si	V	Zn	Fe
wt. / %	0,02	0,1 - 0,2	0,2 - 0,4	0,1	5,8 - 6,8	0,2	0,05 - 0,15	0,1	0,3

Aluminium alloy wire 2319 of 1,2 mm diameter was used for experiments. The chemical composition of the wire is given in Tab. 1. Substrate was aluminium Al 99.5 (series 1050), dimensions 200 mm × 100 mm × 4 mm. The selected process is pulsed MIG, protective gas 70 % argon + 30 % helium, gas flow rate of 18 l/min. The robotic torch angle in relation to the horizontal plane is 90°, and *CTTWD* (Contact Tip To Work Distance) is 15 mm.

The measurement of mean welding current and voltage were performed by instrumentation and software in Fronius, TPS 4000R and were read in remote control unit, RCU 5000i. The measurement of geometric features was carried out by a digital calliper, with a reading scale of 0,01 mm.

2.2 Methods

In this paper, the influence of combination of different travel speed and electric arc power on geometric features of the wall, with an approximately constant heat input along the length of the layer was investigated. Typical wall geometry in cross-section is schematically represented in Fig. 2.

The aims of research are to compare geometric characteristics of produced walls for selected process conditions and to evaluate the uniformity of geometry along the layer length.

Three walls with 15 layers each were made by successively depositing the layers. The layers were deposited in the alternate direction, with the idea of reduction of the difference in geometry from the beginning and the end part of the wall. A time delay is maintained between the layers until the deposited layer cools down to room temperature.

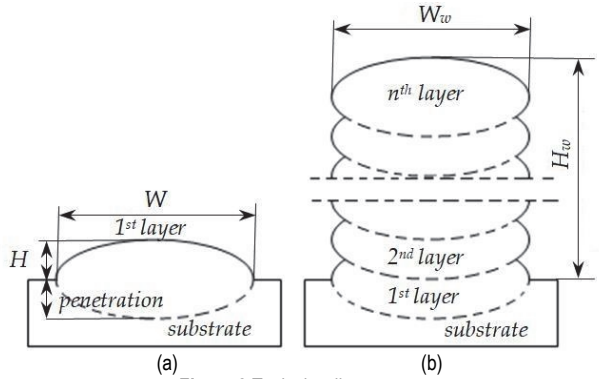

Figure 2 Typical wall geometry
(a) first layer, (b) wall of *n* layers
(*W* - layer width, *H* - layer height, W_w - wall width, H_w - wall height)

The layer paths were created by programming the torch path in four points, as shown in Fig. 3.

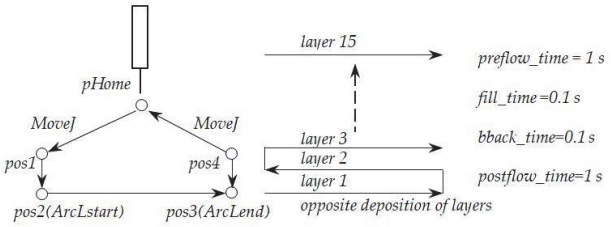

Figure 3 Illustration of the torch path and direction of wall deposition

The interlayer temperature was controlled in a way that the next layer was deposited after the previous one had cooled down to room temperature. After deposition of each layer, the geometry was measured with a digital calliper. For the deposition of the next layer the torch height

position was adjusted for measured mean height of the previous layer in the direction of the +*z* axis.

To achieve uniform geometry of the layer, due to heat properties of aluminium alloy, it is necessary to select different welding current along the layer. At the beginning part of layer when aluminium is cold, the higher heat input related to the middle part must be selected. From the other hand, at the end part of layer, when the aluminium is overheated the lower heat input compared to middle part of layer is recommended. The beginning and the end part are non-stationary regarding the heat flow, but the middle part could be considered as quasi-stationary.

Hence the layer path was divided in three parts, the beginning part, the end part and the middle part with three different heat inputs. The higher heat input in the beginning part of layer was obtained by higher starting current (I_s) of 10 % higher than main current (I) in the middle part of layer. The lower heat input in the end part of layer was selected by lower end current (I_e) of 30 % lower than main current. Transition from starting current to main current and from main current to end current was performed in certain times (t_s, t_e) and slopes (Sl_s, Sl_e), Tab. 3.

Based on measurements and observations of layer uniformity it was decided that the beginning part of 15 mm, the end part of 15 mm are non-stationary and the middle part in length of 150 mm could be considered as quasi-stationary part of the layer.

Wall 1 was experimentally produced at arc travel speed 6 mm/s, wall 2 at 7 mm/s and wall 3 at 8 mm/s, with heat input Q = 265 J/mm ± 5% for the first layer and Q = 217 J/mm ± 5% for layers from 2 to 15, Tab. 2 and Tab. 3.

To ensure sufficient penetration of the deposited wire into the cold substrate, it is necessary to select a higher welding current, i.e. heat input for the first layer compared to the other layers. The heat input per weld length in welding process is defined by the ASME IX QW-409.1 standard, according to the following expression, [30]:

$$Q = \frac{U \cdot I}{TS} \tag{1}$$

where Q is heat input per unit length of weld, J/mm, U is arc voltage, V, I is welding current, A, TS is travel speed, mm/min. Nominal electric arc power (P_n, W) is defined as product of selected arc voltage and selected main current.

Table 2 Selected parameters for quasi-stationary part of walls 1 to 3

Wall No.	Layer No.	TS / mm/s	I / A	U / V	WFS / m/min	$P_n = U \cdot I$ / W	Q / J/mm
1	1.	6	73	21,7	4	1584,1	264,02
	2. - 15.		59	21,3	3,3	1256,7	209,45
2	1.	7	87	22	4,6	1914	273,43
	2. - 15.		73	21,7	4	1584,1	226,3
3	1.	8	93	22,1	4,9	2055,3	256,91
	2. - 15.		79	21,8	4,2	1722,2	215,28
TS - travel speed, I - main current, U - arc voltage, WFS - wire feed speed, P_n - nominal electric arc power, Q - selected heat input per layer length							

Ideally equal heat input values could not be selected due to the synergic selection of arc voltage and welding current over the wire feed speed, which is conditioned by programmed welding power source.

Table 3 Selected parameters at the beginning and the end part of walls 1 to 3

Wall No.	Layer No.	$I_s = 1{,}1 \cdot I$ / A	t_s / s	Sl_s / s	$I_e = 0{,}7 \cdot I$ / A	t_e / s	Sl_e / s
1	1.	80,3	1,5	0,5	51,1	0,1	0,2
	2. - 15.	64,9	1,5	0,5	41,3	0,1	0,2
2	1.	95,7	1,5	0,5	60,9	0,1	0,2
	2. - 15.	80,3	1,5	0,5	51,1	0,1	0,2
3	1.	102,3	1,5	0,5	65,1	0,1	0,2
	2. - 15.	86,9	1,5	0,5	55,3	0,1	0,2
I_s - start current, t_s - duration of I_s, Sl_s - slope of start current, I_e - end current, t_e - duration of Ie , Sl_e - slope of end current							

The measurement of the middle, quasi-stationary part of the layers was performed in 16 measuring points defined at a distance of 10 mm for all 15 layers, Fig. 4. In the beginning and the end part of each layer the measurements were performed in one position, in the middle of starting point and in the middle of the crater. From measured values of the layer widths and heights, the mean values were calculated. For the purpose of findings of local minimum and maximum, the measurements were performed on positions different from position explained in Fig. 4. Those positions were selected in order to investigate the occurrence of bead humping.

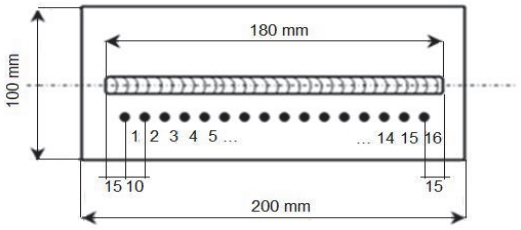

Figure 4 Measurement points for layer heights and widths in the middle part of layer

In this study, a 3D model was created in the SolidWorks 2023 software based on the results of wall geometry measurements, Fig. 5. The 3D model was designed with the assumption of width symmetry, although some small deviations from the actual wall geometries could be expected.

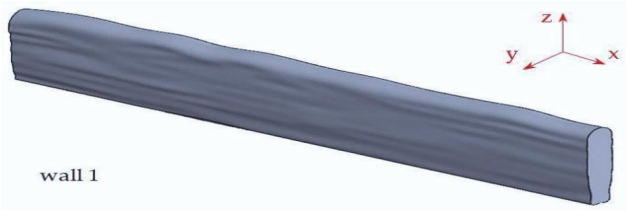

Figure 5 3D model of multi-layered wall 1

This software was used to calculate wall volume according to the generated models.

The deposition efficiency (η_V, %) is calculated as the ratio of the effective wall volume to the molten wire deposition volume, as follows:

$$\eta_V = \frac{V_{weff}}{V_{wire}} \cdot 100\% \tag{2}$$

where V_{weff} is effective volume of the wall, mm^3, V_{wire} is volume of deposited metal wire, mm^3.

Effective wall volume is the volume which could be machined with uniform geometry. Effective wall volume and volume of deposited metal wire were calculated as:

$$V_{weff} = H_{weff} \cdot W_{weff} \cdot L \tag{3}$$

$$V_{wire} = A_{wire} \cdot l_{wire} \tag{4}$$

$$A_{wire} = \frac{\pi \cdot D^2}{4} \tag{5}$$

where H_{weff} is minimum usable wall height, mm, W_{weff} is minimum usable wall width, mm, L is length of quasi-stationary part of the wall (150 mm). A_{wire} is cross-sectional area of the wire, mm^2, l_{wire} is length of deposited metal wire (calculated as the product of wire feed speed and arc duration), mm, D is wire diameter, mm.

The surface wall waviness (*SWI*, mm) was calculated based on the following expression:

$$SWI = \frac{A_{wm} - A_{weff}}{2 \cdot H_{weff}} \tag{6}$$

$$A_{wm} = H_{wm} \cdot W_{wm} \tag{7}$$

$$A_{weff} = H_{weff} \cdot W_{weff} \tag{8}$$

where A_{wm} is mean cross-sectional area of the wall, mm^2, A_{weff} is minimum usable cross-sectional area of the wall, mm^2, H_{wm} is mean usable wall height, mm, W_{wm} is mean usable wall width, mm.

One of the goals of the production of parts using additive technology is the production with the highest possible deposition efficiency and the lowest surface waviness index. The analysis of geometric characteristics and observed phenomena in the process for this selected approach are described in the next chapter.

3 RESULTS AND DISCUSSION

This chapter describes the results of experiments, the measurements and the analysis of geometric features of walls deposited by the application of three arc travel speeds and arc power at approximately constant heat input.

3.1 The Influence of Different Travel Speeds and Arc Power on Wall Geometry at Constant Heat Input

Real welding parameters that were measured during WAAM process are shown in Tab. 4 and Tab. 5. Mean electric arc power (P_m) is calculated as product of mean welding current (I_m) and mean voltage (U_m), without taking process efficiency into account.

Calculated heat inputs per layer length (Q_m) for the first layer deviated for maximum up to −3,18%. The value of Q_m for layers 2 to 15 in quasi-stationary part deviated for maximum up to −4,48%. The synergic way of selecting parameters in programmed welding power source is the reason for that difference between the measured and selected parameters.

Table 4 Measured parameters of WAAM process for the first layer

Wall No.	*TS* / mm/s	Layer part	I_m / A	U_m / V	*WFS* / m/min	$P_m = U_m \cdot I_m$ / W	Q_m / J/mm
1	6	*S*1	81	20,9	4,3	1692,9	282,15
		*S*2	72	21,3	4	1533,6	255,6
		*S*3	45	20,9	2,8	940,5	156,75
2	7	*S*1	100	21,2	5,1	2120	302,86
		*S*2	88	21,2	4,6	1865,6	266,51
		*S*3	56	21,2	3,2	1187,2	169,6
3	8	*S*1	106	21,3	5,3	2257,8	282,26
		*S*2	95	21,3	4,9	2023,5	252,94
		*S*3	60	21,4	3,4	1284	160,5

*S*1 - the beginning part of layer, *S*2 - middle part of layer, *S*3 - the end part of layer, I_m - mean welding current, U_m - mean welding voltage, P_m - mean electric arc power, Q_m - mean heat input per layer length

Table 5 Measured parameters of WAAM process for 2nd to 15th layer

Wall No.	*TS* / mm/s	Layer part	I_m / A	U_m / V	*WFS* / m/min	$P_m = U_m \cdot I_m$ / W	Q_m / J/mm
1	6	*S*1	67,71	19,91	3,6	1348,1	224,63
		*S*2	57,29	20,96	3,3	1200,8	200,07
		*S*3	35,14	20,5	2,3	720,4	119,98
2	7	*S*1	83,5	20,15	4,3	1682,5	242,7
		*S*2	71,5	21,54	4	1540,1	220,04
		*S*3	36,71	21,24	2,8	779,7	111,39
3	8	*S*1	90,64	20,21	4,6	1831,8	229,01
		*S*2	78,07	21,23	4,2	1657,4	210,4
		*S*3	47,93	21,24	2,9	1018	128,09

3.1.1 The Geometry of the First Layer

The geometry of the first layer is different in relation to the other layers due to stronger influence of heat dissipation of the substrate. With each subsequent layer, the influence of the substrate is reduced, and therefore the wall geometry changes.

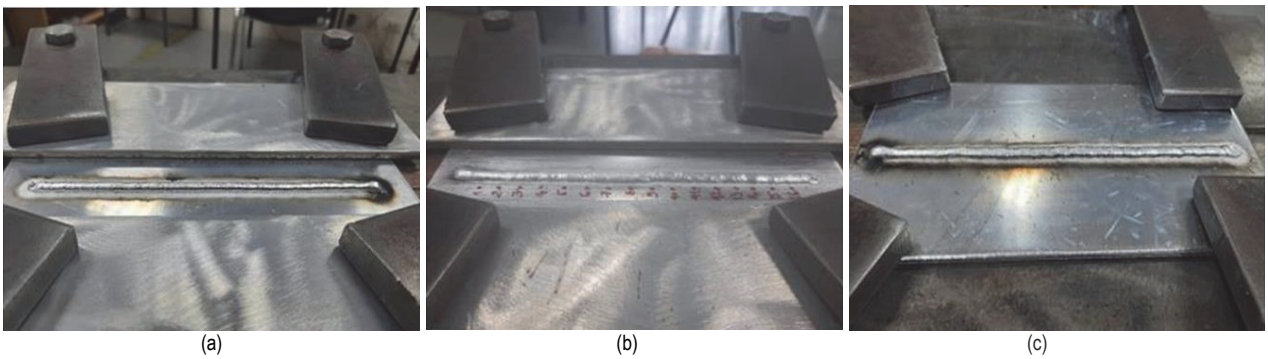

(a) (b) (c)

Figure 6 The first layers of walls
(a) *wall 1*, (b) *wall 2* , (c) *wall 3*

Fig. 6 shows the geometry of the first layer for three walls. For wall 1, the geometry of the first layer is relatively uniform, while for wall 2 and wall 3, irregularities are observed in the form of undulations of the geometry along the deposited layer.

Fig. 7 shows the first layer geometry for all three walls and selected parameters according to Tab. 2. H_m presents mean layer height and W_m is mean layer width. If the travel speed and arc power are increased, layer height is decreased. Also, the layer width increases with increasing travel speed and arc power. According to selected conditions, the width of the first layer for wall 2 is increased by 27,5% relative to wall 1. The width of the first layer of wall 3 is additionally increased by 2,27% compared to a wall 2, or totally 30,4% compared to wall 1.

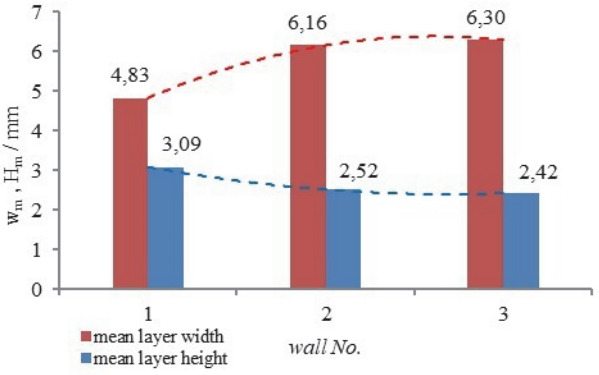

Figure 7 Mean geometry of first layer of quasi-stationary part

Also, the height of the wall 2 first layer is reduced by 18,4% compared to the wall 1, and the height of the wall 3 first layer was further reduced by 3,97%.

3.1.2 The Geometry of Walls

The measured geometric features of the wall 1 to 3 are shown in Tab. 6, which refer to mean values of layer width and height deposited with selected travel speeds, arc power and a relatively constant heat input per layer length.

From the measured values, the minimum widths and heights for each layer were determined of which the smallest values were selected as effective values (W_{eff}, H_{eff}). For example, for the wall 1, the effective wall width is 4.45 mm (for 15 layers, the minimum layer widths in mm are: 4,45; 4,93; 5,51; 6,01; 6,47; 6,4; 6,82; 6,62; 6,69; 6,81; 6,84; 6,79; 6,98; 6,85; 6,66). The effective wall 1 height is (21,95 mm), which is measured in 15th layer. Similarly, for the wall 2 the effective wall width is 5,3 mm, and the effective wall height is (21,17 mm). For the wall 3, the effective wall width is 5,63 mm and the effective wall height is (18,69 mm), Tab. 7.

Fig. 8 shows the dependence of mean wall geometry (from 2nd to 15th layer) to selected travel speeds. For higher arc travel speeds wall height decreased from 21,18 to 19,12. Similar observation could be stated for the first layer, Fig. 7. Also, the layer width increases with increasing travel speed from value 6,8 mm to 7,73 mm and then it decreases slightly for a travel speed of 8 mm/s.

Table 6 Mean layer geometry for selected travel speeds and arc power (data for 1st to 15th layer)

Wall No.	Mean layer width/ layer height	Layer number															
		1.	2.	3.	4.	5.	6.	7.	8.	9.	10.	11.	12.	13.	14.	15.	Avg.
1	W_m / mm	4,83	5,44	5,87	6,43	6,72	7,07	7,12	7,08	6,95	7,04	7,09	7,08	7,24	7,15	6,97	6,67
	H_m / mm	3,09	1,88	1,82	1,44	1,64	1,37	1,62	1,33	1,71	1,21	1,6	1,38	1,67	1,29	1,51	1,64
2	W_m / mm	6,16	5,74	6,51	7,26	7,56	8,04	8,14	8,06	8,08	8,22	8,28	8,28	8,04	7,95	8,01	7,62
	H_m / mm	2,52	1,95	1,38	1,3	1,5	1,28	1,47	1,29	1,2	1,32	1,56	1,3	1,38	1,51	1,3	1,48
3	W_m / mm	6,30	5,88	6,4	6,95	7,26	7,52	7,72	7,97	7,85	8,07	8,11	8,23	8,06	7,82	7,84	7,47
	H_m / mm	2,42	1,91	1,49	1,45	1,29	1,23	1,35	1,5	1,29	0,85	1,48	1,04	1,64	1,19	1,43	1,44
W_m - mean layer width, H_m - mean layer height																	

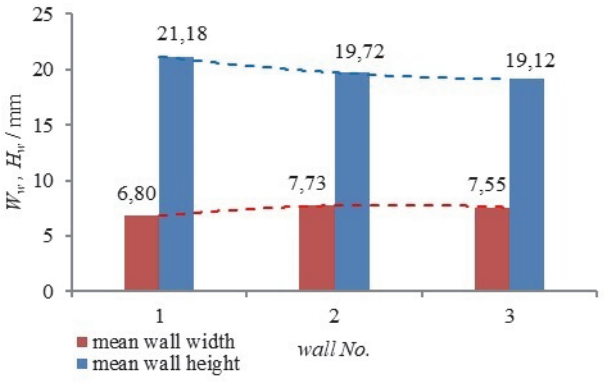

Figure 8 Mean geometry for quasi-stationary part of walls 1 to 3 (2nd to 15th layer)

As can be seen in Fig. 9, three selected arc travel speeds and combinations of process parameters resulted in different waviness. The main reason for this phenomenon can be explained by the relationship between travel speed and welding current. The appearance of "hills" and "valleys" is clearly visible and more pronounced at a travel speed of 7 mm/s and especially at TS of 8 mm/s. This phenomenon with irregular geometry can be observed from the 5th layer, and it progressively increases up to the 15th layer of the wall 3 (Fig. 9g, Fig. 9h, Fig. 9i)).

Correlation of the mean layer height (H_m) (2nd to 15th) to the number of deposited layer (n_l) of the wall is presented in Fig. 10. Excluding the first layer due to the previously explained reason, the highest mean layer height was achieved for wall 1 (1,88 mm), and the lowest mean layer height for wall 3 (0,85 mm). Then, the average layer heights of walls are: for wall 1, 1,53 mm, for wall 2, 1,41 mm and for wall 3, 1,37 mm.

It could be stated that higher arc travel speed and higher arc power with constant heat input per layer length result in lower mean layer height. It is evident from the graph in Fig. 10 that the mean layer heights are stabilized after 3rd and 4th layer for walls 1 and 2, but for wall 3 mean layer heights are more irregular. Cycling of mean layer heights (lower-higher-lower) could be attributed to the repeatedly changing of direction of layer deposition.

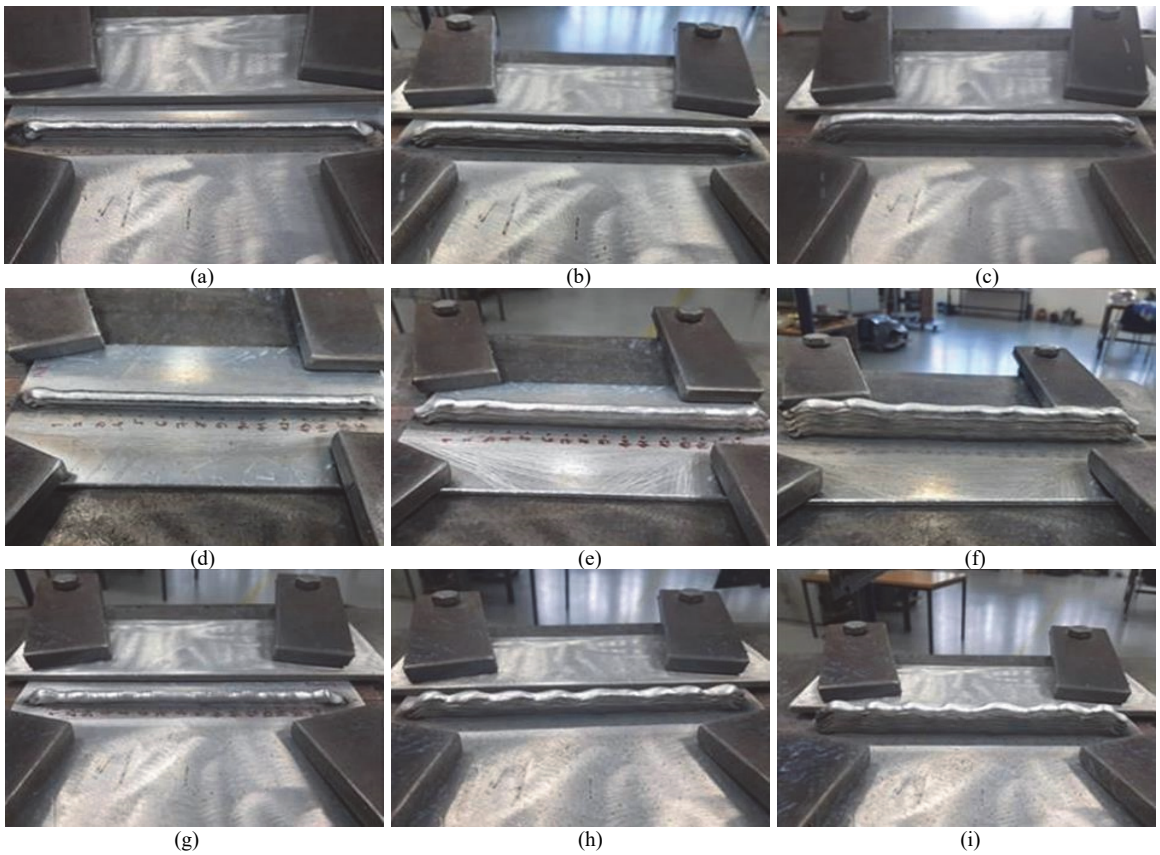

Figure 9 Geometry of walls:
wall 1 - (a) 5th layer; (b) 10th layer; (c) 15th layer
wall 2 - (d) 5th layer; (e) 10th layer; (f) 15th layer
wall 3 - (g) 5th layer; (h) 10th layer; (i) 15th layer

It is interesting to analyse the standard deviation of layer heights (σ_H) to get clear information to the wall quality, Fig. 11. It is obvious that a geometric profile with a lower height deviation per layer length was achieved with lower arc travel speed (6 mm/s, wall 1).

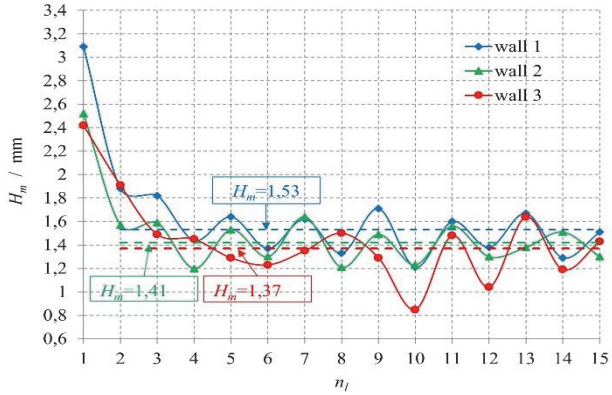

Figure 10 Correlation of mean layer height to the number of wall layers
(The data in rectangles are mean layer heights from 2nd to 15th layer)

For the wall 3, the standard deviation of the layer height (σ_H) takes on the highest values and increases with the deposition of the next layers.

Arc travel speed of 8 mm/s (wall 3) resulted in excessive wall waviness even after five deposited layers, Fig. 9h. Such geometry can be described as humping. Humping can be encountered in WAAM. In that case it causes the problem regarding the bead geometry and regular part realisation [20]. Maximum difference of layer height of "hills" and "valleys" for the wall 1 is 1,05 mm, for the wall 2 is 2,6 mm and for the wall 3 maximum difference is 3,98 mm, Fig. 12.

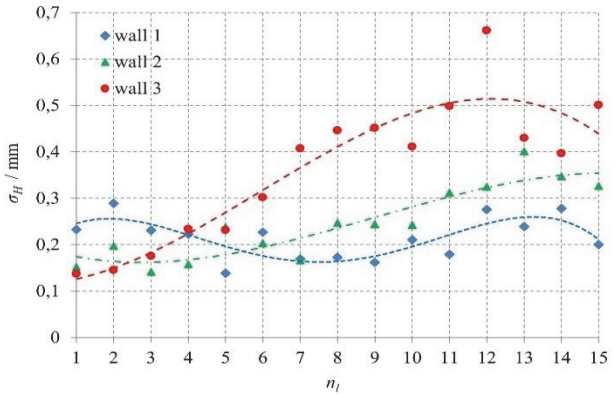

Figure 11 Standard deviation of wall layer heights

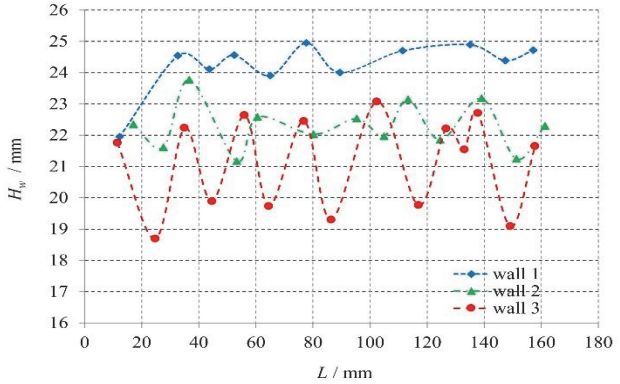

Figure 12 Distribution of wall height at positions of bead humping

After the analysis of layer height, the similar principle is applied for the analysis of layer width. The correlation between mean layer width (W_m) and number of layers (n_l) is presented in Fig. 13.

The layer width is stabilized between 6th and 8th layer for all three walls, as can be seen in Fig. 13. The layers width for walls 1 and 2 is stabilized after the 6th layer, and for wall 3 after the 8th layer.

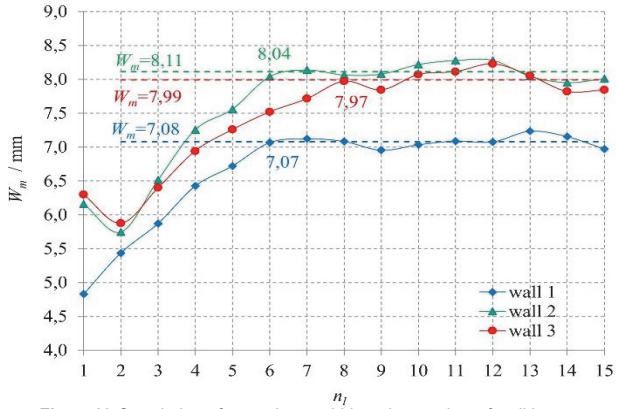

Figure13 Correlation of mean layer width to the number of wall layer

Although encountered in hybrid laser-MIG additive technology, it could be stated similar trend of layer width can be observed, where the layer width of deposited aluminium alloy 5356 stabilizes after 5 to 6 layers [18].

The standard deviation of layers width (σ_W) for each individual layer is shown in Fig. 14. The largest layer width deviation along the individual layers is observed for the wall 3, and the deviation increases with the increase in the number of layers. The standard deviation of the layer width has the smallest changes for the wall 1.

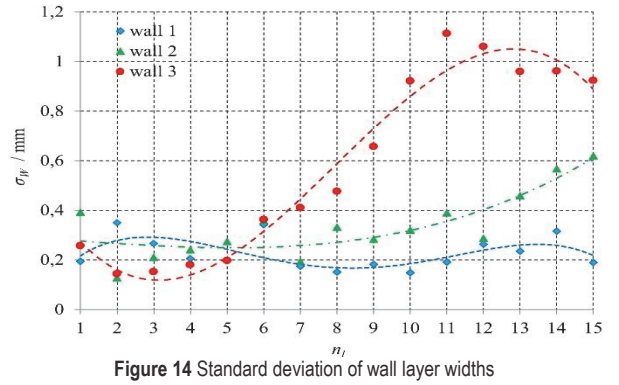

Figure 14 Standard deviation of wall layer widths

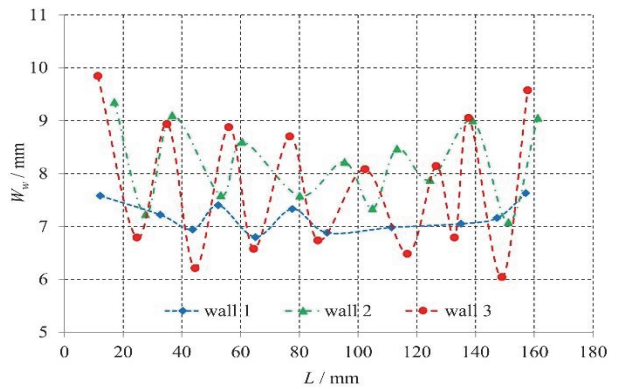

Figure 15 Distribution of wall width in 15th layer at positions of bead humping

The waviness of the wall width is also important factor in analysis of stability of the wall geometry. More significant waviness of layer width (W_m) was observed for the wall 2 and especially for the wall 3, Fig. 15.

Maximum difference of layer width of "hills" and "valleys" for the wall 1 is 0,83 mm, for the wall 2 is 2,27 mm and for the wall 3 the maximum difference is 3,53 mm.

In further research, an analysis of the efficiency of depositing the wall was carried out, from the point of view of volume efficiency. The results of the analysis are presented in the next chapter.

3.2 The Deposition Efficiency and Surface Waviness of Walls

The deposition efficiency (η_V) is calculated according to Eq. (2) and using volumes of walls from models created in SolidWorks 2023 (Fig. 5, Fig. 16) and from Tab. 7. *SWI* is calculated according to Eq. (6).

In this study, the highest volume deposition efficiency (70,11%) and the lowest *SW* index of 1,29 mm (calculated according to Eq. (6) to Eq. (8)) were achieved for wall 3 (Tab. 7). The volume deposition efficiency of wall 1 is 61,9 %, and for wall 2 it is 68.85%. The values for H_{weff} and W_{weff} were obtained in the way previously described in subsection 3.1.2. Calculated *SWI* were from 1,29 mm to 1,35 mm.

Some authors calculate the deposition efficiency as the ratio of effective and total cross-sectional area [17], while other authors calculate with the ratio of effective and total deposited volume [18], which is more acceptable. Deposition efficiency using aluminium alloy wire of 1,2 mm diameter achieved by MIG process was 75,04 %, achieved with aluminium alloy 5356, which is comparable to the deposition efficiency achieved in this work. In addition, a significant surface quality factor in additive manufacturing is the surface waviness index (*SWI*), and for the given conditions with aluminium alloy AlMg5, was achieved between 0,3 mm and 0,5 mm [20]. If we consider the paper [16], using CMT, CMT-ADV and CMT-PADV process with aluminium alloy 5556, *SWI* from 0,89 mm to 1,4 mm were achieved, defined as half the difference between the maximum and effective wall width. Deposition efficiencies were in the range 73 - 80%. To achieve geometric accuracy, it is necessary to achieve the highest possible deposition efficiency and the lowest possible *SW* index.

The explanation of the achieved geometric features in this research is given in the following analysis. From previous results and analysis, it is observed that despite better visual geometry of wall 1, higher deposition efficiencies are observed for wall 2 and especially for wall 3. That is because the minimum layer width among all three walls is associated with the wall 1, 4,45 mm. Also, an indicator of deposition quality is the mass that needs to be machined, which is the highest (25,57 g) for the wall 1. Trend of deposition efficiency is accompanied with the same trend of surface waviness index which is the best for wall 3 (*SWI* = 1,29 mm) followed by the wall 2 (*SWI* = 1,33 mm) and finally by wall 1 (*SWI* = 1,35 mm).

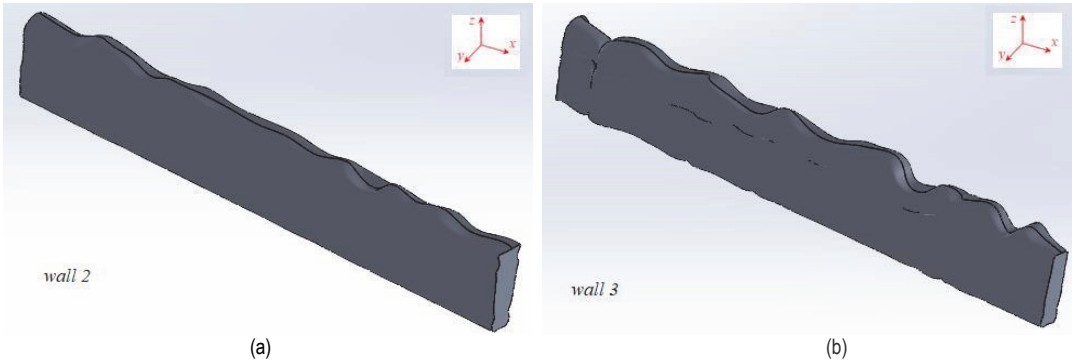

(a) (b)

Figure16 3D models of multi-layered wall 2 (a) and wall 3 (b)

Table 7 Calculated volumes and deposition efficiencies of walls (1st to 15th layer)

Wall no.	H_{weff} / mm	W_{weff} / mm	A_{weff} / mm	V_{weff} / mm^3	V_{wire} / mm^3	V_{model} / mm^3	ΔV / %	η_V / %	m_{wire} / g	m_{eff} / g	Δm / g	SWI / mm
1	21,95	4,45	97,68	14 651,63	23 656,19	24 211,27	2,35	61,94	67,18	41,61	25,57	1,35
2	21,17	5,3	112,2	16 830,15	24 444,86	25 142,87	2,86	68,85	69,42	47,8	21,62	1,33
3	18,69	5,63	105,22	15 783,7	22 513,44	23 739,84	5,45	70,11	63,94	44,82	19,12	1,29

H_{weff} - effective wall height, W_{weff} - effective wall width, A_{weff} - effective wall cross-sectional area
V_{weff} - effective volume of the quasi-stationary part, V_{wire} - deposited volume
V_{model} - wall volume calculated from 3D models, ΔV - difference of model volume and deposited volume
η_V - volume deposition efficiency, m_{wire} - mass of wire
m_{eff} - effective mass of the wall, Δm - mass that needs to be machined
SWI - surface waviness index

3.3 The Beginning and the End of the Wall Layers

If the beginning and the end parts of the walls are considered, a geometric deviation from the quasi-stationary part of the wall is observed, Fig. 17. Measurements of the geometry of the initial and final part of the layer were performed approximately in the middle of the slope from the edge to the transition into the quasi-stationary part of the layer (approximately 15 mm). According to quasi-stationary part of the walls, the differences are significant both in the height and in the width of the measured segment, which is numerically shown in Tab. 8. Due to significant geometric differences at both ends, it is necessary to further optimize the process parameters with the aim of achieving a uniform geometry.

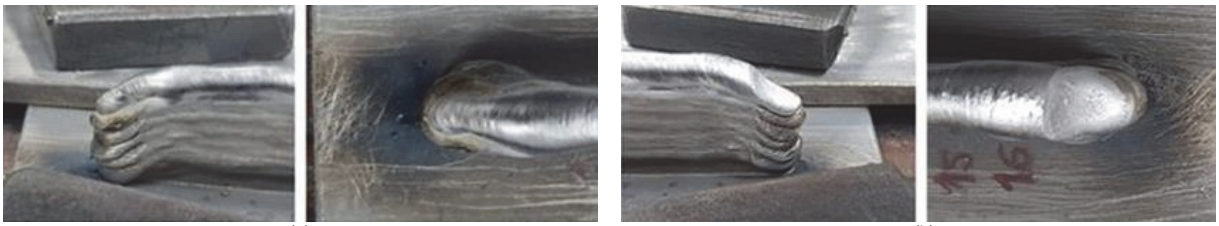

(a) (b)

Figure 17 The beginning (a) and the end part (b) of the completed wall 1

Table 8 Geometric differences of the beginning and the end part to quasi-stationary part of the 15th layer

Wall no.	H_{st} / mm	H_{wm} / mm	H_{et} / mm	W_{sm} / mm	W_{wm} / mm	W_{em} / mm	ΔH_s / %	ΔH_e / %	ΔW_s / %	ΔW_e / %
1	18,6	24,59	19,95	5,48	6,67	8,26	24,3	18,8	17,8	28,9
2	17,85	22,61	16,95	5,99	7,62	9,04	21,05	25,03	21,4	18,6
3	18,3	21,52	16,8	6,61	7,47	8,68	14,9	21,9	11,5	16,2

H_{st} - total wall height at the beginning part, H_{wm} - mean wall height at quasi-stationary part
H_{et} - total wall height at the end part, W_{sm} - mean width of layers at the beginning part
W_{wm} - mean wall width at quasi-stationary part, W_{em} - mean width of layers at the end part
ΔH_s - difference between total wall height at the beginning part and quasi-stationary part
ΔH_e - difference between total wall height at the end part and quasi-stationary part
ΔW_s - difference between mean layers width at the beginning part and quasi-stationary part
ΔW_e - difference between mean layers width at the end part and quasi-stationary part

Analysis of the geometry of the wall at both ends shows differences in width and height per layer. In the beginning part of the layers, a different geometry occurs compared to quasi-stationary part due to the excessive accumulation of material in the arc ignition phase, which results in a larger geometric profile. Geometric errors in the beginning part became more significant with further deposition of layers. The difference in geometry in the crater occurs due to the lack of molten metal in the arc extinguishing phase. Related to quasi-stationary part, the differences of height in the beginning part were from 14,9% to 24,3%, and in the end part of the wall height differences were from 18,8% to 25,03%. The differences between mean layer width at the beginning part and middle part were from 11,5% and 21,4%, and the mean layer width differences at the end part were from 16,2% to 28,9%.

4 CONCLUSIONS

The main goal of this research was the application of WAAM technology on single-pass, multi-layer straight walls on aluminium alloy 2319 using p-MIG process. The bidirectional deposition strategy of wall forming was used with constant heat inputs and variable electric arc travel speeds and power. The walls consisted of 15 layers and first layer was produced with higher heat input than other layers. Heat input for first layer was 265 J/mm ± 5% and 217 J/mm ± 5% for all subsequent layers. Detailed process data are referenced in Tab. 2 and Tab. 3. The analysis was performed for quasi-stationary part and for both ends of wall.

Based on this research, the following conclusions were reached:

- Deposition efficiencies were from 61,94% to 70,11% (wall 1 and wall 3). Efficiency of wall 2 was 68,85%.
- Second wall quality indicator, SWI, was almost identical for all 3 walls (from 1,29 mm to 1,35 mm).
- Despite the same heat input with different process parameters, different wall geometries were achieved.
- The geometry of the first layer affects the wall deposition efficiency and was different for three walls. The lowest standard deviation is for wall 1 for layer width 0,19 mm and layer height 0,23 mm compared to other two walls.
- It can be generally concluded that for all three walls the layer width stabilizes after 6th to 8th layers. The layer height stabilization is achieved after 4th layers for the walls 1 and 2 but wall 3 exhibited constant variations throughout all 15 layers.
- Wavy longitudinal geometry (along *x* axe) was especially accentuated on the final layer of wall 3, where significant humping is evident. Maximum difference between "hills" and "valleys" was 3,98 mm and is significantly higher when compared to wall 2 (2,6 mm) or wall 1 (1,05 mm).
- There was a significant deviation of the wall geometry at the beginning and end wall parts compared to the part of the wall produced under thermal quasi-stationary condition. Deviation of wall height at both end was from 14,9% to 25,03%. Deviation of wall width at both end was from 11,5% to 28,8%.
- 3D models created upon frequent real measurement have proven to be a useful tool in the representation of actual walls for the calculation of the volumes and deposition efficiency.

Further research and optimization of the starting and finishing WAAM process parameters to produce uniform geometry along the entire wall profile for aluminium alloy 2319 is necessary and recommended.

Acknowledgement

The authors thank the Faculty of Electrical Engineering, Mechanical Engineering and Naval Architecture for providing the equipment for experimental work.

5 REFERENCES

[1] ISO/ASTM 52900:2021 (E) (2021). Additive manufacturing - General principles - Fundamentals and vocabulary. ASTM International, West Conshohocken, PA.

[2] González, J., Rodríguez, I., Prado-Cerqueira, J. L., Diéguez, J. L., & Pereira, A. (2017). Additive manufacturing with GMAW welding and CMT technology. *Procedia Manufacturing, 13*, 840-847. https://doi.org/10.1016/j.promfg.2017.09.189

[3] Ding, D. (2015). *Process planning for robotic wire ARC additive manufacturing. Doctor of Philosophy, School of Mechanical*. Materials and Mechatronics Engineering, University of Wollongong, Australia.

[4] Derekar, K. (2018). A review of wire arc additive manufacturing and advances in wire arc additive manufacturing of aluminium. *Materials Science and Technology, 34*, 8, 895-916. https://doi.org/10.1080/02670836.2018.1455012

[5] Ding, D., Pan, Z., Cuiuri, D., & Li, H. (2015). Wire-feed additive manufacturing of metal components: technologies, developments and future interests. *The International Journal of Advanced Manufacturing Technology, 81*, 465-481. https://doi.org/10.1007/s00170-015-7077-3

[6] Bendia, R. M., Lizarralde, F., & Coutinho. F. G. (2021). Multivariable closed-loop control for layer geometry in Wire-Arc Additive Manufacturing. *XV Simpósio Brasileiro de Automação Inteligente*, 1278-1283. https://doi.org/10.20906/sbai.v1i1.2732

[7] Chergui, M. A. (2021). *Simulation Based Deposition Strategies Evaluation and Optimization in Wire Arc Additive Manufacturing*. Doctor of Philosophy, Université Grenoble Alpes, France.

[8] Shah, A., Aliyev, R., Zeidler, H., & Krinke, S. (2023). A Review of the Recent Developments and Challenges in Wire Arc Additive Manufacturing (WAAM) Process. *Journal of Manufacturing and Materials Processing, 7*(3), 97. https://doi.org/10.3390/jmmp7030097

[9] Jafari, D., Vaneker, T. H. J., & Gibson, I. (2021). Wire and arc additive manufacturing: Opportunities and challenges to control the quality and accuracy of manufactured parts. *Materials & Design, 202*(1), https://doi.org/10.1016/j.matdes.2021.109471

[10] Stinson, H., Ward, R., Quinn, J., & Mc Garrigle. C. (2021). Comparison of Properties and Bead Geometry in MIG and CMT Single Layer Samples for WAAM Applications. *Metals, 11*(10), 1530. https://doi.org/10.3390/met11101530

[11] Yildiz, A. S., Davut, K., Koc, B., & Yilmaz, O. (2020). Wire arc additive manufacturing of high-strength low alloy steels: study of process parameters and their influence on the bead geometry and mechanical characteristics. *Int. J. Adv. Manuf. Technol*., 108, 3391-3404. https://doi.org/10.1007/s00170-020-05482-9

[12] Novelino, A. L. B., Carvalho, G. C., & Ziberov. M. (2022). Influence of WAAM-CMT deposition parameters on wall geometry. *Advances in Industrial and Manufacturing Engineering, 5*, 100105. https://doi.org/10.1016/j.aime.2022.100105

[13] Arana, M., Ukar, E., Rodriguez, I., Aguilar, D., & Álvarez, P. (2022). Influence of deposition strategy and heat treatment on mechanical properties and microstructure of 2319 aluminium WAAM components. *Materials & Design, 221*, https://doi.org/10.1016/j.matdes.2022.110974

[14] Wei, Y., Liu, F., Liu, Fe., Yu, D., You, Q., Huang, C., Wang, Z., Jiang, W., Lin, X., & Hu. X. (2023). Effect of arc oscillation on porosity and mechanical properties of 2319 aluminium alloy fabricated by CMT-wire arc additive manufacturing. *Journal of Materials Research and Technology, 24*, 3477-3490. https://doi.org/10.1016/j.jmrt.2023.03.203

[15] Greebmalai, J. & Warinsiriruk, E. (2020). Multi-Heat Input Technique for Aluminium WAAM Using DP-GMAW Process. *AIP Conference Proceedings, 2279*, 050001, 2-7. https://doi.org/10.1063/5.0022954

[16] Gierth, M., Henckell, P., Ali, Y., Scholl, J., & Bergmann, J.

P. (2020). Wire Arc Additive Manufacturing (WAAM) of Aluminium Alloy AlMg5Mn with Energy-Reduced Gas Metal Arc Welding (GMAW). *Materials, 13*(12), 2671. https://doi.org/10.3390/ma13122671.

[17] Lee, H. K., Kim, Ja., Pyo, C., & Kim, Ji. (2020). Evaluation of Bead Geometry for Aluminium Parts Fabricated Using Additive Manufacturing-Based Wire-Arc Welding. *Processes, 8*, 1211, 1-14. https://doi.org/10.3390/pr8101211

[18] Zhang, Z., Sun, C., Xu, X., & Liu, L. (2018). Surface quality and forming characteristics of thin-wall aluminium alloy parts manufactured by laser assisted MIG arc additive manufacturing. *International Journal of Lightweight Materials and Manufacture, 1*(2), 89-95. https://doi.org/10.1016/j.ijlmm.2018.03.005

[19] Nguyen, T. C., Weckman, D. C., Johnson, D. A., & Kerr, H. W. (2006). High speed fusion weld bead defects. *Science and Technology of Welding and Joining, 11*(6), 618-633. https://doi.org/10.1179/174329306X128464

[20] Wu, D., Hua, X., Ye, D., & Li, F. (2017). Understanding of humping formation and suppression mechanisms using the numerical simulation. *International Journal of Heat and Mass Transfer, 104*, 634-643, https://doi.org/10.1016/j.ijheatmasstransfer.2016.08.110

[21] Yehorov, Y., da Silva, J. L., & Scotti, A. (2019). Balancing WAAM Production Costs and Wall Surface Quality through Parameter Selection: A Case Study of an Al-Mg5 Alloy Multilayer-Non-Oscillated Single Pass Wall. *Journal of Manufacturing and Materials Processing, 3*, 32, 1-19, https://doi.org/10.3390/jmmp3020032

[22] Jurisic, Z. & Krnic, N. (2022). Prediction of weld geometry of AlMg3 sheets using artificial neural networks with different input data sets. *Proceedings of the 10th International Scientific and Expert Conference (TEAM2022)*, 109-117, ISSN 1847-9065, Slavonski Brod, Croatia.

[23] Xiong, J., Yin, Z., & Zhang, W. (2016). Forming appearance control of arc striking and extinguishing area in multi-layer single-pass GMAW-based additive manufacturing. *International Journal of Advanced Manufacturing Technology, 87*, 579-586. https://doi.org/10.1007/s00170-016-8543-2

[24] Wang, Z., Zimmer-Chevret, S., Léonard, F., & Abba, G. (2022). Improvement strategy for the geometric accuracy of bead's beginning and end parts in wire-arc additive manufacturing (WAAM) *International Journal of Advanced Manufacturing Technology, 118*(1), 2139-2151. https://doi.org/10.1007/s00170-021-08037-8

[25] Waqas, A., Qin, X., Xiong, J., Wang, H., & Zheng, Ch. (2019). Optimization of Process Parameters to Improve the Effective Area of Deposition in GMAW-Based Additive Manufacturing and its Mechanical and Microstructural Analysis. *Metals, 9*(7), 775. https://doi.org/10.3390/met9070775

[26] Gomez Ortega, A., Corona Galvan, L., Deschaux-Beaume, F., Mezrag, B., & Rouquette. S. (2018). Effect of process parameters on the quality of aluminium alloy Al5Si deposits in wire and arc additive manufacturing using a cold metal transfer process. *Science and Technology of Welding and Joining, 23*(4), 316-332. https://doi.org/10.1080/13621718.2017.1388995

[27] Xiong, J., Zhang, Y., & Pi, Y. (2021). Control of deposition height in WAAM using visual inspection of previous and current layers. *Journal of Intelligent Manufacturing, 32*, 2209-2217. https://doi.org/10.1007/s10845-020-01634-6

[28] Wang, Z., Zimmer-Chevret, S., Léonard, F., & Abba, G. (2022). Control of bead geometry using multiple model approach in wire-arc additive manufacturing (WAAM). *International Journal of Advanced Manufacturing Technology, 122*, 2939-2951, https://doi.org/10.1007/s00170-022-10053-1

[29] Welding Consumables - Product Catalogue (2019). Lincoln Electric. https://www.lincolnelectric.com.

[30] ASME BPV Code, Section IX, 2019 Edition, (2019). ASME International, https://www.asme.org/.

Contact information:

Živko JURIŠIĆ, MSc, B. Sci. Mech. Eng.
(Correspoding author)
Croatian Military Academy
Zrinsko-Frankopanska 207 a, Split, Croatia
E-mail: zivko.jurisic2015@gmail.com

Nikša KRNIĆ, PhD, Assoc. Prof.
Faculty of Electrical Engineering,
Mechanical Engineering and Naval Architecture (FESB),
University of Split, 21000, Ruđera Boškovića 32, Split, Croatia
E-mail: nkrnic@fesb.hr